 CMES, vol.77, no.2, pp.81-111, 2011

Modeling Two Phase Flow in Large Scale Fractured Porous Media with an Extended Multiple Interacting Continua Method

A.B. Tatomir [1] [2], A.Szymkiewicz [3], H. Class [1] and R. Helmig [1]

Abstract: We present a two phase flow conceptual model, the corresponding simulator (2pMINC) and a workflow for large-scale fractured reservoirs, based on a continuum fracture approach which uses the multiple interacting continua (MINC) method complemented with an improved upscaling technique. The complex transient behavior of the flow processes in fractured porous media is captured by subgridding the coarse blocks in nested volume elements which have effective properties calculated from the detailed representation of the fracture system. In this way, we keep a physically based approach, preserve the accuracy of the model, avoid the common use of empirically derived transfer functions and considerably reduce the complexity of the problem which is reflected in the speedup factors up to 1000. The results are verified by comparison to a discrete fracture model (DFM) for which the fractures and matrix are explicitly accounted for. The simulator is applied to an idealized medium with periodic fracture pattern and to a real, naturally fractured reservoir, mapped on the "wave platforms" along the Bristol Channel. The evaluation shows that the extended MINC model is able to reproduce both, the large-scale permeability and the dynamics of the fracture-matrix mass transfer, correctly.

Keywords: fractured porous media simulator, upscaling and reservoir simulation, MINC, double-porosity model

[1] University of Stuttgart, Department of Hydromechanics and Modeling of Hydrosystems, Pfaffenwaldring 61, 70569 Stuttgart, Germany

[2] Author for correspondence (E-mail:alexandru.tatomir@iws.uni-stuttgart.de,Tel:+4971168564712)

[3] Gdańsk University of Technology, Faculty of Civil and Environmental Engineering, Narutowicza 11/12, 80233, Gdańsk, Poland

Symbol	Definition	Unit
Latin Letters:		
$k_{r\alpha}$	relative permeability of phase α	[-]
$\mathbf{K}$	intrinsic permeability	$[m^2]$
p	pressure	$[Pa]$
p_c	capillary pressure	$[Pa]$
p_d	entry pressure	$[Pa]$
q_α	source or sink term of the phase α	$[m^3/(m^3 s)]$
S_α	saturation of phase α	[-]
$S_{\alpha r}$	residual saturation of phase α	[-]
t	time	$[s]$
T^{ij}	coarse scale transmissibility between node i and j	$[m^3]$
$T^i_{k,k+1}$	inner block i transmissibility between continuum k and $k+1$	$[m^3]$
Greek Letters:		
α	phase n or w	
λ	empirical constant from the Brooks-Corey p_c relationship related to the pore size distribution	
λ_α	phase α mobility	
μ	dynamic viscosity	$[Pa\ s]$
∇_{FF}	coarse-scale operator (interactions between the fracture blocks solved at global scale)	
∇_{MM}	fine-scale operator (interactions inside the coarse block between the matrix continua solved at the local scale)	
ϕ	total porosity	[-]
ρ	fluid density	$[kg/m^3]$
Subscripts:		
n	non-wetting phase related quantity	
w	wetting phase related quantity	

1 Introduction

Fracture systems have been investigated for more than 60 years in different fields like hydrology, petroleum engineering, or geothermal energy and, currently, a wide literature is available. Many engineering applications present a very high interest in the correct simulation of multiphase flow in fractured porous media, for example, oil recovery [Lemonnier and Bourbiaux (2010); Kazemi (1976)], CO_2 storage in geological formations [Carneiro (2009); Kopp, Class, and Helmig (2009)], nuclear waste storage [Bodvarsson, Boyle, Patterson, and Williams (1999)], remediation of contaminated aquifers [Berkowitz (2002); Niessner, Helmig, Jakobs, and Roberts (2005)] etc. Extensive literature reviews can be found in [Berkowitz (2002); Neuman (2005); Reichenberger, Jakobs, Bastian, and Helmig (2006); Karimi-Fard, Durlofsky, and Gong (2006); Assteerawatt (2008); Geiger, Cortis, and Birkholzer (2010)]. As fractures occur on a variety of length scales and in a variety of problems, the fracture flow models have been roughly classified in discrete fracture models (DFM), continuum fracture models (CFM) and hybrid models (i.e [Berkowitz (2002)]) which are a combination of the previous two. The DFMs consider the fractures explicitly and therefore require huge data density and computation power, whereas CFMs require the determination of a representative elementary volume (REV), the appropriate effective parameters and transfer functions between continua. For a large scale problem, like a CO_2 storage reservoir, there could be millions of fractures which might have to be considered which could be a formidable task for a DFM simulator. In this sense, a very common approach among the CFMs is to consider the reservoir as dissociated into two interacting continua, fracture and matrix, linked with a transfer term, which does not require the fine discretization of the DFM or the detailed fracture characterization during simulations. This is called the dual- or double- porosity (DP) model and was introduced by Barenblatt, Zheltov, and Kochina (1960) and Warren and Root (1963) (Fig. 1 (2)).

The classical DP model suffers from several limitations which have been identified in e.g. Pruess and Narasimhan (1982); Zimmerman, Hadgu, and Bodvarsson (1996); Karimi-Fard, Durlofsky, and Gong (2006); Unsal, Matthäi, and Blunt (2009); Geiger, Cortis, and Birkholzer (2010) . The method works best if the fracture network is sufficiently well connected, and the difference between the permeabilities is large. We enumerate some of the approximations of the classical DP model: the flow between the fracture and matrix, which is called the inter-porosity flow, is quasisteady; it neglects flow in the matrix and the spatial variation within the matrix blocks; it uses empirical transfer functions for the complex fracture-matrix interactions; it uses average properties for the fracture network which cannot capture its complexity in a permeability tensor; and it lacks a clear procedure to determine the parameters from a particular discrete fracture system. Several

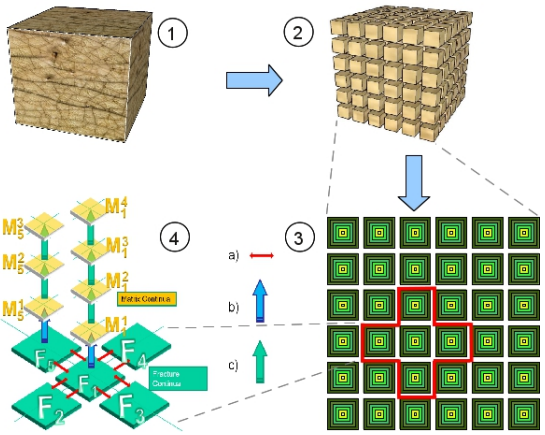

Figure 1: 1) Fractured reservoir with 2) schematic representation of the MINC model (3D) and 3) a 2D crossection through the "sugar cube model" 4) showing the connectivities: a) coarse-block inter-connectivity or fracture-fracture; b) fracture-matrix c) matrix-matrix connections.

approaches try to determine improved transfer functions that accurately represent the matrix-fracture exchange [Zimmerman, Chen, Hadgu, and Bodvarsson (1993); Abushaikha and Gosselin (2009)] or to quantify the equivalent effective parameters (equivalent fracture permeabilities and matrix block dimensions) [Zimmerman and Bodvarsson (1995),Min, Jing, and Stephansson (2004)]. For oil recovery, Abushaikha and Gosselin (2009) proposes a so-called "SubFace" transfer function that accurately simulates the exchange of fluid between fracture and matrix by capillary imbibition and gravity drainage and they compare it with the conventional, the non-conventional and the improved transfer functions. Another approach to resolve matrix dynamics is to introduce subgridding e.g. [Pruess and Narasimhan (1982), Karimi-Fard, Durlofsky, and Gong (2006)]. The *multiple interacting continua* (MINC) method belongs to the CFM category and is an approximate method for modeling fluid and heat flow in fractured porous media developed by Pruess and Narasimhan (1982). Pruess (1992) gives a brief guide to the MINC-method for modeling flow and transport in fractured porous media. The method is a generalization of the double porosity concept but treats the inter-porosity flow in a fully transient way. If the fracture network is sufficiently connected, shortly after a perturbation has occurred, some of the regions will have the same or almost the same thermodynamic properties (pressure, saturation, temperature, etc.) which means that these flow areas can be lumped together into distinct continua. The classical MINC approach assumes that the thermodynamic properties of the matrix vary with

the distance from the nearest fracture or, in other words, the equipotential surfaces are equally distanced from the nearest fracture. This leads to the partitioning of the flow domain into computational volume elements where all interfaces between the volume elements are parallel to the nearest fracture, similar to a matryoshka nesting doll. Fig. 1 shows the basic idea of this method. Conceptually similar models, where the flow in matrix blocks is resolved at fine scale, were developed for double porosity media using asymptotic homogenization [Douglas and Arbogast (1990); Lewandowska, Szymkiewicz, Burzynski, and Vauclin (2004)]. However, the key aspect of the MINC method remains, as in every DP model, the estimation of the effective permeabilities and, in addition to that, the subdivisions of the matrix domain. The classic concept is using the idealized representation of the fractured reservoir (i.e. sugar cube model) and the inter-porosity flow parameters are calibrated at a later time. In the recent years, the hydraulic and geologic description of fractured reservoirs has progressed considerably. Therefore, if sufficient information is available regarding the fracture distribution in the studied reservoir, the upscaled parameters have to be determined based on the underlying geometry of the fractures. Neglecting them and using the same transfer terms for the whole domain might lead to less accurate results. The aim is to benefit from the complexity of the DFMs and the computational simplicity of the CFMs. For instance, Bourbiaux, Cacas, Sarda, and Sabathier (1997) present a method to derive the equivalent block sizes and to compute the equivalent permeabilities from single-phase, steady-state flow computations by using a 3D resistor network method and specific boundary conditions. Later on, Sarda, Jeannin, Basquet, and Bourbiaux (2002) developed, from the double-porosity model, an optimized explicit representation of the fractured medium by assigning a matrix volume to the nearest fracture, according to the distance. Basquet, Bourbiaux, and Cohen (2005) proposes a homogenization procedure on a discrete fracture network to reduce the number of fracture nodes from the model of Sarda, Jeannin, Basquet, and Bourbiaux (2002), while keeping the same hydraulic properties. Unsal, Matthäi, and Blunt (2009) describe a multiphase flow fracture-only simulator where they model the fracture geometry explicitly and the inter-porosity flow by using empirical transfer functions. Similar approaches of using subgridding techniques were proposed by Naimi-Tajdar, Han, Sepehrnoori, Arbogast, and Miller (2007), who developed a parallel simulator for large-scale naturally fractured reservoirs based on the MINC method. Zyvoloski, Robinson, and Viswanathan (2008) developed a MINC-type model where the number of subgrid blocks associated with a coarse block varies in space. Famy, Bourbiaux, and Quintard (2005) proposes an improvement to the subgridding technique so that it predicts more accurately the matrix-fracture exchanges. Karimi-Fard, Durlofsky, and Gong (2006) introduced an upscaling methodology as an extension to the previous MINC subgridding procedure, which derives the effective parameters from

detailed fracture characterization (i.e. the subgrids are constructed for each coarse block using the isopressure curves obtained from local pressure solutions of a DFM over the block). Some of the main problems regarding the upscaling of fractured reservoirs are summarized in Vitel and Souche (2007). They argue that the boundary conditions imposed on a coarse block do not consider the dynamic behavior further away from the block, which may constitute a source of error. The standard upscaling approaches are facing difficulties in dealing with the entry pressure effects. In the context of a new emerging field of application, i.e. CO_2 storage in geological formations, this research extends the applicability range investigated by Karimi-Fard, Durlofsky, and Gong (2006); Gong, Karimi-Fard, and Durlofsky (2008) by considering non-wetting phase migration in a saturated wetting domain.

The goal of this work is the development of a workflow that allows the study of multiphase flow in fractured reservoirs based on the improved MINC approach with the upscaling procedure proposed by Karimi-Fard, Durlofsky, and Gong (2006), that includes a conceptual model and a numerical simulator. The paper is structured as follows: the next section describes the mathematical and numerical model of the extended MINC model; Section 3 will introduce the workflow followed by some numerical experiments, and finally, by the conclusions.

2 Model Concepts

2.1 General two-phase flow equations

The conservation of mass in a multiphase flow context can be written for each fluid phase α as follows:

$$\frac{\partial(\phi S_\alpha \rho_\alpha)}{\partial t} + \nabla \cdot (\mathbf{v}_\alpha \rho_\alpha) - \rho_\alpha q_\alpha = 0 \tag{1}$$

where the velocity v_α is given by the extended expression of Darcy's law to multiphase flow:

$$v_\alpha = -\frac{k_{r\alpha}}{\mu_\alpha}\mathbf{K} \cdot (\nabla p_\alpha - \rho_\alpha g) \tag{2}$$

After inserting Eq. 2) in Eq. 1) the general two-phase flow equations for porous media are obtained [Helmig (1997)]:

$$\frac{\partial(\phi S_\alpha \rho_\alpha)}{\partial t} - \nabla \cdot \left(\frac{\mathbf{K} k_{r\alpha}}{\mu_\alpha} \rho_\alpha (\nabla p_\alpha - \rho_\alpha g) \right) - \rho_\alpha q_\alpha = 0 \tag{3}$$

2.2 Constitutive relationships

The constitutive relationships in fracture and matrix domains can be formulated according to Brooks and Corey (1964) who proposed the following relationship for the effective saturation:

$$S_e = \frac{S_w - S_{wr}}{1 - S_{wr}} = \left(\frac{p_d}{p_c}\right)^{\lambda} \tag{4}$$

The relative permeability is a parameter that accounts for the increased resistance to flow for a given phase due to the presence of the other phase. The Brooks-Corey model is applied together with the Burdine theorem:

$$\begin{aligned} k_{rw} &= S_e^{\frac{2+3\lambda}{\lambda}} \\ k_{rn} &= (1-S_e)^2\left(1 - S_e^{\frac{2+\lambda}{\lambda}}\right) \end{aligned} \tag{5}$$

The coupling between saturation and pressure is achieved with the closing relations:

$$\begin{aligned} S_w + S_n &= 1 \\ p_n - p_w &= p_c \end{aligned} \tag{6}$$

2.3 DFM model

The DFM will be used as a reference solution for the extended MINC model. The construction of this model starts with a common assumption that Darcy's law is valid for fractures, which allows us to use Eq. 3 for both matrix and fracture domains. The fractures are represented as lower-dimensional entities (1-D lines in 2-D domain). Any heterogeneity supposes a sudden change in the rock properties (permeability, porosity etc.). This means that across the fracture-matrix interfaces there might appear a discontinuity in the primary variables (saturation and pressure), which can be solved by introducing an interface condition. The *extended capillary pressure-saturation interface condition* (e.g. Reichenberger, Jakobs, Bastian, and Helmig (2006); Niessner, Helmig, Jakobs, and Roberts (2005)) proposed by Duijn, Molenaar, and Neef (1995) is going to be used. Its first requirement is the fluid conservation. The second requirement is the continuity of the intensive state variables, like the capillary pressure, which can be only achieved if there is a discontinuity in the saturation.

2.4 Extended MINC model

2.4.1 Basic equations

The coarse-scale model is described by equations with the general form like Eq. 3): for fracture continuum (F):

$$\frac{\partial(\phi S_\alpha \rho_\alpha)_F}{\partial t} - \nabla_{FF} \cdot \left(\frac{\mathbf{K}^{eff} k_{r\alpha}}{\mu_\alpha} \rho_\alpha (\nabla p_\alpha - \rho_\alpha \mathbf{g}) \right)_F - (\rho_\alpha q_\alpha)_F - \tau_{FM} = 0, \tag{7}$$

for matrix continua (M_k) with $k = \overline{1, \mathscr{K}}$:

$$\frac{\partial(\phi S_\alpha \rho_\alpha)_{M_k}}{\partial t} - \nabla_{MM} \cdot \left(\frac{\mathbf{K}^{eff} k_{r\alpha}}{\mu_\alpha} \rho_\alpha (\nabla p_\alpha - \rho_\alpha \mathbf{g}) \right)_{M_k} - (\rho_\alpha q_\alpha)_{M_k} + \tau_{FM} = 0, \tag{8}$$

The transfer term, τ_{FM} is the exchange between the matrix and the fracture and is governed by the solution of the local matrix flow equation. $(K^{eff})_{M_k}$ represents the effective (upscaled) matrix permeability of continua M_k.

2.4.2 Upscaling procedure

In most of the double-porosity models and the classical MINC approach there is no systematic procedure to determine the effective parameters from the DFM. One typical way to determine the parameters is to construct the "sugar-cube" model and calibrate it to the field tests. In order to improve the accuracy of the classical MINC method by means of better accounting for the spatial variability of the matrix blocks, and of the dynamics within the blocks an upscaling methodology has been developed by Karimi-Fard, Durlofsky, and Gong (2006) as an extension to the previous MINC subgridding procedure. The upscaling procedure can be summarized to the following steps.

- To determine the internal block transmissibilities between the nested volume elements, a single phase compressible flow equation is solved considering no-flow boundary conditions and the flow exchange is calculated between fracture network and matrix (Fig. 2a).
- The upscaled inter-block transmissibilities are determined using a two-point approximation technique by setting a permeameter-type boundary condition for every two neighboring coarse cells and solving again a steady state one phase flow equation (Fig. 2b).

Before starting the description of the upscaling procedure the following assumptions have to be considered:

- the fracture network is sufficiently well connected throughout the considered fractured porous domain;
- if there are regions with reduced connectivity, these do not have to be predominant even though the upscaling procedure can be applied for limited zones.

2.4.3 Intra-coarse-block transmissibilities

The determination of the fracture network and matrix connections and those within a coarse block between the nested volume elements (Fig. 1 (4) a) and c)) is made by solving a compressible single-phase flow equation with the DFM for each individual coarse block:

$$\phi \frac{\partial \rho}{\partial t} - \nabla \cdot \left(\frac{\rho \mathbf{K}}{\mu} \nabla p \right) = q, \tag{9}$$

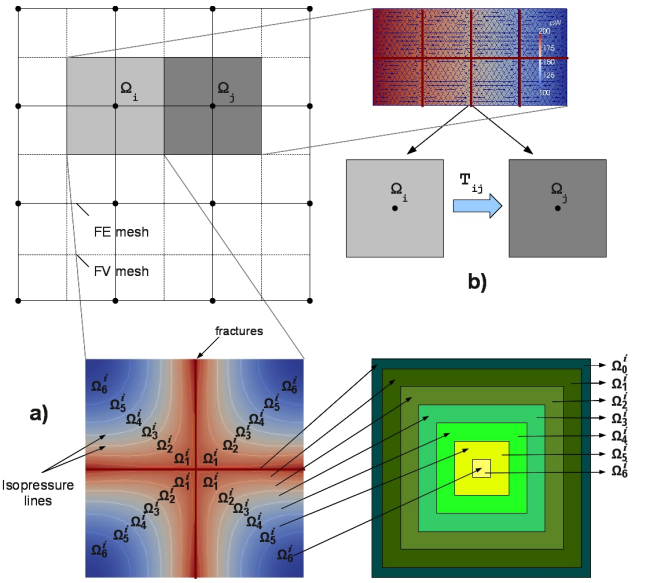

Figure 2: Vertex centered finite volume discretization of the coarse scale model showing coarse blocks Ω_i and Ω_j a) Pressure profile and iso-pressure lines at quasi-steady state for local block Ω_i represented at fine-scale and the construction of the idealized sugar-cube block's nested volume elements $\Omega_1^i, \Omega_2^i, ..., \Omega_6^i$; b) Inter-coarse-block transmissibility T_{ij} determination (i.e. between coarse block Ω_i and Ω_j)

The boundary conditions of the isolated coarse block are set to no-flow everywhere while there is a constant injection rate in the connected fracture network. The pressure in the block will increase and will reach a pseudo-steady state where the change of the ratio $\frac{\partial \rho}{\partial t}$ is smaller than a certain threshold ($1e-02$ for our case), so that it can be considered constant. The pressure in the fracture network is approximately the same and in the matrix it has a diffusion like profile. Fig. 2a illustrates a square block with two perpendicular fractures that is the fine scale representation of the coarse block Ω^i with the resulting isopressure line profiles. This coarse block is used in Section 4 to determine the effective parameters for the idealized periodic fracture reservoir examples. The pressure profile is independent of the injection rate and of the fluid properties. It depends only on the fracture network geometry and on porous matrix properties. Using the isopressure lines resulted from the pressure solution we can determine the volume of each nested volume element and the transmissibilities between them, which are going to be used by the MINC model. We calculate first the minimum and maximum pressures in the coarse-block, Ω^i, p^i_{min}, respectively, p^i_{max} and we subdivide this interval into $\mathscr{K}$, which is the number of nested volume elements, or continua, of the coarse-block. The subregions located in between these isopressure curves are usually not connected to each other and do not overlap. Their union designates the coarse block:

$$\Omega^i = \bigcup_{k=1}^{\mathscr{K}} \Omega^i_k. \tag{10}$$

Depending on the pressure value resulted from the fine-scale single-phase solution, each vertex is assigned to one of the $\mathscr{K}$ subregions. The bulk volume of each subregion, V^i_k, is calculated by summing up all the vertex centered volumes within that subregion:

$$V^i_k = \sum_{j \in \Omega^i_k} V_j. \tag{11}$$

The average porosity of subregion is also calculated with:

$$\overline{\phi}^i_k = \frac{\sum_{j \in \Omega^i_k} V_j \phi_j}{\sum_{j \in \Omega^i_k} V_j} \tag{12}$$

The mass accumulation within a subregion is:

$$A^i_k = \sum_{j \in \Omega^i_k} V_j \phi_j \frac{\partial \rho_j}{\partial t}, \tag{13}$$

and can also be expressed as the difference between the flow in and out of the subregion, i:

$$A_k^i = Q_{k-1,k}^i - Q_{k,k+1}^i. \tag{14}$$

For the last subregion, $\mathscr{K}$, Eq. 14 becomes:

$$A_{\mathscr{K}}^i = Q_{\mathscr{K}-1,\mathscr{K}}^i. \tag{15}$$

Starting with the last subregion we calculate the mass flow rates between subregions, $Q_{k,k+1}^i$, and the inner-block transmissibilities, accordingly:

$$T_{k,k+1}^i = \frac{Q_{k,k+1}^i \mu}{\overline{\rho}_k^i \left(\overline{p}_k^i - \overline{p}_{k+1}^i\right)} \tag{16}$$

where $\overline{p}_k^i$ is the average pressure in the subregion.

2.4.4 Inter-coarse-block transmissibilities

The transmissibilities between the coarse blocks (Fig. 1 subfigure(4)a and Fig. 2b) are calculated with a two point upscaling technique. The setup shown in Fig. 2b considers two adjacent coarse blocks i and j taken together, with the upper and lower boundaries set to no-flow and a pressure gradient from left to right boundaries, which are Dirichlet. The flux $Q^{i,j}$ between the two blocks is calculated over their interface. The transmissibility results:

$$T^{i,j} = \frac{Q^{i,j}\mu}{\overline{\rho}\left(\overline{p}^i - \overline{p}^j\right)}. \tag{17}$$

In the above procedures the transmissibilities only depend on the coarse discretization. The capillary pressures and the relative permeabilities are used directly from the fine-scale to the coarse-scale.

2.4.5 Discretization Scheme - Vertex Centered Finite Volume Method

The geometrical complexity of the fracture network systems, kept intact in the DFMs, imposes the utilization of unstructured grids as spatial discretization. The numerical scheme to be used has to take into account the unstructured grids and the sharp fronts that can occur between the fracture and the matrix. This imposes the utilization of the locally mass conservative method, the vertex centered finite volume method (VCFVM) which is also found in literature under the name of subdomain collocation finite volume method or box method (Helmig (1997), Reichenberger, Jakobs, Bastian, and Helmig (2006)). For the MINC method the same

VCFVM is used considering this time the structured grid (Fig. 2a). The time discretization for both models is a first order fully-implicit backward Euler scheme which generates a large non-linear system of equations. These systems are linearized using the Newton-Rhapson method. Considering the vector of gravitation $\mathbf{g} = (0,0,g)$ to act only in the vertical direction the total potential can be formulated: $\Psi_\alpha = p_\alpha - \rho_\alpha g z$, where z is the geodetic height. The discretized form of the two-phase flow equations for extended MINC method can be written for the fracture continuum as:

$$\begin{aligned}
&\left(\left(S_{\alpha,F^i}\phi_{F^i}\rho_{\alpha,F^i}\right)^{t+\Delta t} - \left(S_{\alpha,F^i}\phi_{F^i}\rho_{\alpha,F^i}\right)^{t}\right)\frac{|V_T^i|}{\Delta t} \\
&+ \sum_{l\in E_i}\sum_{j\in\eta_i}\frac{1}{2}\lambda_{\alpha,i,j}^{FU_l}T^{ij}\left(\Psi_{\alpha,F^i}^{t+\Delta t} - \Psi_{\alpha,F^j}^{t+\Delta t}\right) \\
&- q_{\alpha,F^i}^{t+\Delta t}|V_T^i| - \lambda_{\alpha,F^i,M_1^i}^{FU}T_{F^i,M_1^i}^{i}\left(p_{\alpha,F^i}^{t+\Delta t} - p_{\alpha,M_1^i}^{t+\Delta t}\right) = 0,
\end{aligned} \tag{18}$$

where E_i is the set of elements l which have vertex i as a corner, η_i is the set of nodes j neighboring node i that share a subcontrol volume edge with the control box V_T^i, $|V_T^i|$ is the volume of the control volume (box) corresponding to node i. Indices t and Δt stand for the time discretization and $\lambda_{\alpha,i,j}$ is the mobility term of the phase $\alpha = w,n$. We use the fully upwind (FU) finite volume method for the mobilities. Term $1/2$ is introduced as the flux between block i and j is equally splitted between the two subcontrol volumes that share edge ij. They add up to unity after computing the sums over elements. As for the matrix continuum M_k^i, the discretized flow equations in the interior of the coarse block i are:

$$\begin{aligned}
&\left(\left(S_{\alpha,M_k^i}\overline{\phi}_{M_k^i}\overline{\rho}_{\alpha,M_k^i}\right)^{t+\Delta t} - \left(S_{\alpha,M_k^i}\overline{\phi}_{M_k^i}\overline{\rho}_{\alpha,M_k^i}\right)^{t}\right)\frac{|V_{M_k}^i|}{\Delta t} \\
&- \lambda_{\alpha,M_k^i,M_{k+1}^i}^{FU}T_{k,k+1}^{i}\left(p_{\alpha,M_k^i}^{t+\Delta t} - p_{\alpha,M_{k+1}^i}^{t+\Delta t}\right) \\
&+ \lambda_{\alpha,M_{k-1}^i,M_k^i}^{FU}T_{k-1,k}^{i}\left(p_{\alpha,M_{k-1}^i}^{t+\Delta t} - p_{\alpha,M_k^i}^{t+\Delta t}\right) = 0
\end{aligned} \tag{19}$$

and for the last matrix continuum, M_K^i:

$$\begin{aligned}
&\left(\left(S_{\alpha,M_K^i}\overline{\phi}_{M_K^i}\overline{\rho}_{\alpha,M_K^i}\right)^{t+\Delta t} - \left(S_{\alpha,M_K^i}\overline{\phi}_{M_K^i}\overline{\rho}_{\alpha,M_K^i}\right)^{t}\right)\frac{|V_{M_K}^i|}{\Delta t} \\
&+ \lambda_{\alpha,M_{K-1}^i,M_K^i}^{FU}T_{K-1,K}^{i}\left(p_{\alpha,M_{K-1}^i}^{t+\Delta t} - p_{\alpha,M_K^i}^{t+\Delta t}\right) = 0
\end{aligned} \tag{20}$$

3 Workflow

The numerical simulation of multiphase flow in fractured porous media is constructed on several modules which interact as shown in Fig. 3. This kind of flow

chart can also be encountered for other applications and it is not necessarily specific to fracture flow alone. However, fractured reservoirs differ from other systems due to an increased level of geometric complexity, reflected in the necessity of using unstructured grids and adaptive meshing. This, in turn implies higher complexity for code development and for computation.

We will first introduce the modeling system and later we will describe the simulation environment components.

3.1 DuMu^x modeling system

DuMu^x is a free and open-source simulator for flow and transport processes in porous media developed on the Distributed and Unified Numerics Environment (DUNE). A description of the DuMu^x modeling system, its capabilities, together with an overview on software related aspects is given in Flemisch, Darcis, Erbertseder, Faigle, Lauser, Mosthaf, Müthing, Nuske, Tatomir, Wolff, and Helmig (2011), Flemisch, Fritz, Helmig, Niessner, and Wohlmuth (2007). DuMu^x and DUNE consist of a series of modules which can be combined loosely to achieve the best characterization of the problem. The previously described two phase fracture flow models, DFM and MINC model, are implemented in DuMu^x under the names, `2pDFM` and `2pMINC` and belong to the so called *extended models* category [Flemisch, Darcis, Erbertseder, Faigle, Lauser, Mosthaf, Müthing, Nuske, Tatomir, Wolff, and Helmig (2011)]. The approach used at their implementation is fully implicit and fully coupled.

3.2 Geometric modeling

The first step in the modeling system is to generate the domain geometry. In real life applications, information about the exact location of each individual fracture is most probably unknown. This challenging step of obtaining a reasonable approximation of the fracture network system is often done with a fracture generator. `FRAC3D` is a two- and three-dimensional fracture generator, developed by Hemminger (2002) and Assteerawatt (2008) which offers three different approaches: deterministic, statistic and geo-statistic fracture generation. The domains created have "*.art*" or "*.bnd*" extensions. The "*.art*" file format consists of three parts: a) *Vertices* which have the cartesian coordinates on x, y, z directions; b) *Edges* having a boundary id, an id of the first node and an id of the second node. The fractures are specified with negative boundary ids; c) *Faces* having the face id and the boundaries which belong to each face. In case the geometric information about the fracture system is provided in a file format common to the commercial simulators (e.g. CAD, Rhino, ICEM) there are several file format converters which allow conversions in both directions.

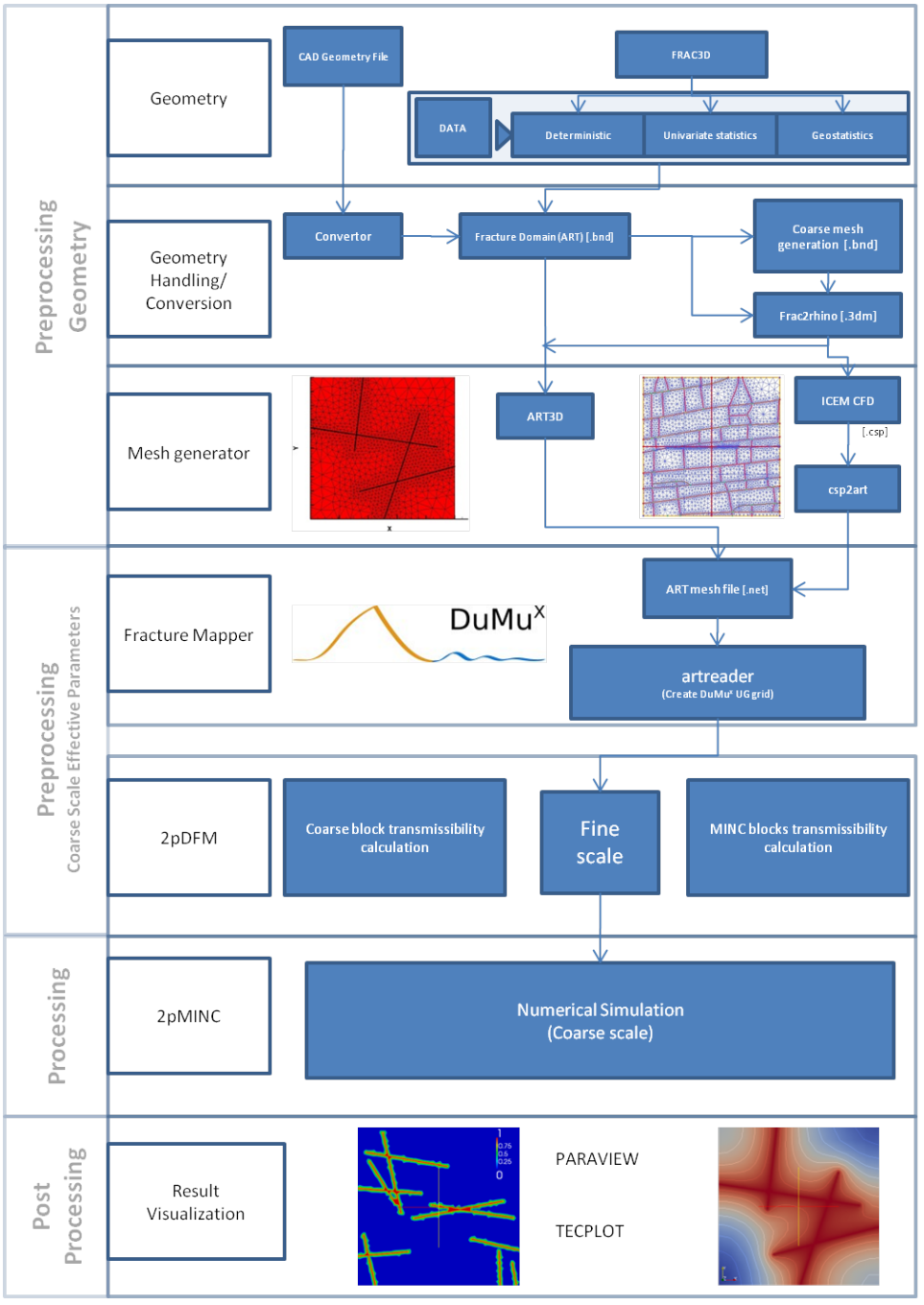

Figure 3: Schematic description of the modeling system

The second step is to generate the grid from the domain "*.art*" file. Several automatic grid generators can be used (e.g. `ART3D` developed by Fuchs (2001), or the commercial ICEM from Ansys). The lower dimensional fracture model has the advantage of fast grid generation compared to the equi-dimensional concept where the fractures are represented as thin layers. In the same time, adaptive grid generation prevents the creation of an unreasonably large number of elements. `ART3D` allows adaptive meshing for both lower and equi-dimensional fracture geometries. Having the discrete fracture network geometry earlier obtained either with the geo-statistical fracture generator or directly from field measurements, one intermediate step before the mesh generation can be the overlapping of the coarse grid over the fracture network system then followed by the creation of the fine scale grid over the entire fracture domain (see Fig. 4). This procedure prevents coarse elements to have non-rectangular shapes or to have fine scale finite elements contained in two distinct coarse elements. DUNE allows the use of several grid implementations such as UG

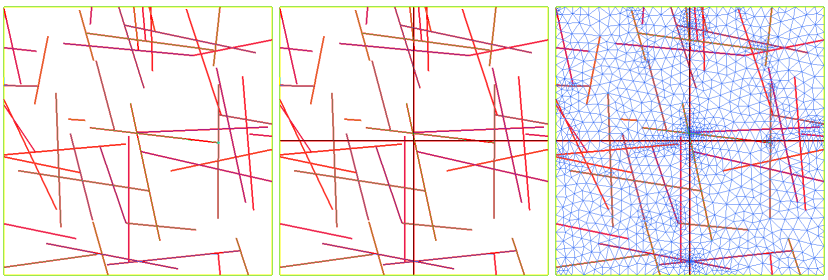

(a) (b) (c)

Figure 4: Exemplification for fine and coarse scale grid construction for the whole fractured reservoir. Fracture pattern obtained with the geo-statistical fracture generator FRAC3D

[Bastian, Birken, Johannsen, Lang, Neuss, Rentz-Reichert, and Wieners (1997)], Alberta [Schmidt and Siebert (2005)], or ALU-Grid [Dedner (2004)], etc. The automatic grid generation process may lead to creation of poor quality elements. This requires a "mesh quality check" and the correction of those elements. One easy way to perform corrections is by using the automatic "mesh quality check" tool of ANSYS ICEM CFD. The next step after the creation of the grid in DuMu^x is the mapping of the fractures, which are lower dimensional entities and in the same time element edges. A vertex and an edge mapper are constructed, such that they provide the information about each global index of a vertex, or edge, if it is a fracture or matrix. Both pieces of information are stored in two separate vector data structures. This step is essential for the later implementation of the interface conditions

and for the calculation of the flux and storage terms.

3.3 Coarse scale effective parameters

The calculation of the coarse scale effective parameters belongs to the preprocessing stage and consists of solving single phase problems in the shape of Eq. 9 for each coarse block at the fine scale with the `2pDFM` simulator. The procedure is continued as described in Section 2.4.2. Each coarse block of the MINC model is provided with the volumetric fractions and the inner-transmissibilities of the nested volume elements, and with the transmissibilities with the neighboring coarse-blocks. The advantage of this upscaling procedure is that the effective parameters are calculated only once in this preprocessing step, with a rather simple procedure. Now, the flow at the coarse scale can be modeled with the `2pMINC` simulator.

3.4 Postprocessing

The preprocessing steps of geometric modeling, mesh generation and processing and the postprocessing steps of result visualization are loosely coupled to the DuMu^x simulation environment. The results are usually visualized with the open-source, multi-platform data analysis and visualization application ParaView. It is also possible to view the results and grids with Tecplot.

4 Numerical Examples

In this section, we compare the results obtained by explicitly modeling the fractured porous domain with the DFM and the ones obtained with the extended MINC method. In this way, we are able to validate and test the accuracy of the `2pMINC` simulator and to present the individual steps of the modeling process linked to the stages of the workflow. Three examples are presented: the first two examples are considering a simplified idealized representation of a fractured reservoir which are easier to implement and solve; the last one is a real natural fractured reservoir with a high network fracture connectivity. It is worth mentioning that the `2pDFM` flow simulator was compared to other simulators - TOUGH2 and MSFLOW [Wu, Pan, and Pruess (2004)] and MUFTE-UG [Reichenberger, Jakobs, Bastian, and Helmig (2006)] and to published laboratory experimental results from [Kazemi (1976)], who ran a series of laboratory experiments of water imbibition into fractured matrix cores to displace oil. A series of verification studies were performed to test the lower-dimensional DFM with the equi-dimensional one. Here we extend the range of application investigated by Karimi-Fard, Durlofsky, and Gong (2006) who considered oil-recovery applications by injecting water into an oil saturated media, to

non-wetting phase infiltration into a wetting saturated domain. These applications are most valuable for estimating the migration of contaminant in the ground water aquifers, or of the CO_2 storage in geological formations.

4.1 Two phase flow in an idealized periodic fracture system

We consider modeling the migration of a contaminant DNAPL (TCE) through a simple idealized fracture network consisting of a periodic pattern of orthogonal fractures. The resulting enclosed square matrix blocks are 1×1 meters. The whole domain is 20×20 meters and all fractures have the width of $3.91e-04$ meters. The problem description and the material properties are given in Tab. 1. The idealized periodic geometry is rather simple to implement directly as "*.art*" format and therefore it does not require a CAD program for construction or further conversions. In the next preprocessing step, `ART3D` generates a triangular mesh as depicted by Fig. 5.

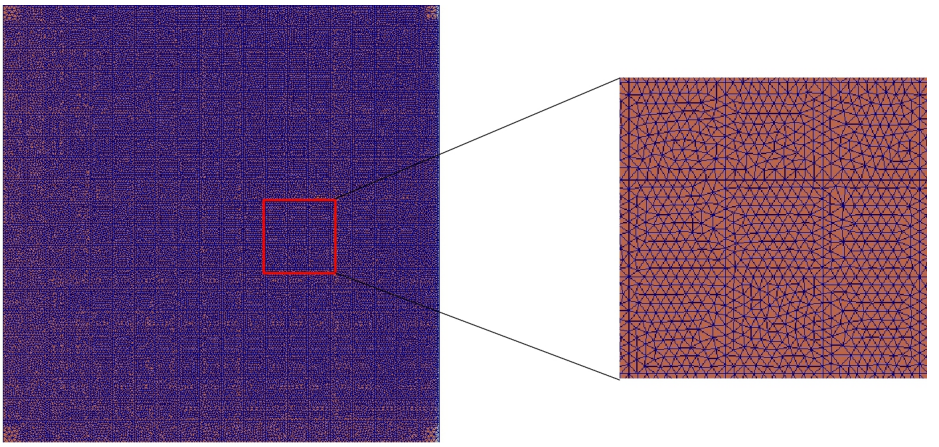

Figure 5: Fine-scale model discretization

4.1.1 Test problem 1: "Permeameter type" experiment

For simplicity, the gravity effects were neglected and the capillary pressure curves and the porosities of the fractures and matrix are chosen to be the same. The relative permeability of the rock matrix is calculated with the Brooks Corey relations (Eq. 4) and a λ exponent of 2, which is a value usually applied to highly nonuniform materials Helmig (1997).

The primary variables are chosen p_w and S_n, so the initial non-wetting saturation is set as $S_n = 0.20$ and a wetting pressure, $p_w = 1.0e{+}05$ $[Pa]$. The boundary conditions

Table 1: Material properties and problem description for "Permeameter type" experiment.

		Domain Properties	
		matrix	**fracture**
Permeability, K	$[m^2]$	$1.0e-15$	$b^2/12$
Eff. porosity, ϕ	[-]	0.5	0.5
Entry pressure, p_d	$[Pa]$	2000	2000
Pore size dist. idx.λ	[-]	2.0	2.0
Residual saturation S_{wr}	[-]	0.01	0.01
Residual saturation S_{nr}	[-]	0.01	0.01
Fracture aperture b	$[m]$	-	$3.915e-4$
		Fluid Properties	
Viscosity Water, μ_w	$[kg/ms]$	$1.0e-3$	
Density Water, ρ_w	$[kg/m^3]$	1000	
Viscosity DNAPL, μ_n	$[kg/ms]$	$5.7e-4$	
Density DNAPL, ρ_n	$[kg/m^3]$	1460	
		Boundary Conditions	
Left[Dirichlet]: p_w , S_n	$[Pa]$, [-]	$p_w = 2.0e+05$	$S_n = 0.80$
Right[Dirichlet]: p_w , S_n	$[Pa]$, [-]	$p_w = 1.0e+05$	$S_n = 0.20$
Top & Bottom [No Flow]			
		Initial Conditions	
p_w , S_n	$[Pa]$, [-]	$p_w = 1.0e+05$	$S_n = 0.2$

are considered similar to a permeameter experiment where the pressure heads are specified at in-and out-flow sections and no flow is occurring through the lateral walls. We fix on the left boundary the p_w = 2.0e+05 $[Pa]$ and the S_n = 0.80, and on the right boundary p_w = 1.0e+05 $[Pa]$ and S_n = 0.20. The top and bottom boundaries are set no-flow.

In the next stage of preprocessing, the calculation of the effective upscaled parameters is performed on coarse blocks of 2×2 meters (Fig. 2a, for the inner-block and two adjacent coarse blocks Fig. 2b), for the inter-coarse-block. The resulting coarse block effective permeability is 5.01e-13 m^2. We choose each coarse block to contain a number of 6 nested volume elements: one fracture continuum and five matrix continua. To make the calculation independent of the choice of the MINC grid size we compute the effective permeabilities instead of the effective transmissibilities. The permeability between the fracture and the matrix continua is calculated as the

harmonic mean.

In the post processing visualization step, the results are presented in terms of non-wetting-saturation profiles along the diagonal (lower left corner to upper right corner) at different times (Fig. 6). All simulations were performed on a processor Intel(R) Core(TM)2 Quad CPU Q9300 @ 2.50GHz and 8GB RAM. Simulation time for `2pDFM` is 15517.6 seconds on a grid with 37269 nodes, and for `2pMINC` on a grid with 121 nodes and 6 nested volume elements is only 421.3 seconds. Fig. 6 illustrates the non-wetting saturation profiles of the two simulations: DFM (upper), MINC (lower) and their plot over the diagonal line (lower left - upper right corners). As, the main flow direction is along the horizontal fractures and perpendicular to the vertical ones, we can distinguish two periods of interest during the simulation. The first one is from the beginning of the non-wetting phase infiltration until it reaches the opposite boundary (Fig. 6 (a-c)), and the second one is the slow increase of non-wetting saturation in the whole domain. The fine-scale reference solution (DFM) is represented by the irregular, "zig-zag" line (SN_2pDFM), where the peaks of the curve result at the point where the diagonal intersects a fracture and the low values are in the center of each matrix block. The continuous lines, named SN_0 to SN_5 are obtained with the MINC model, "0" being the fracture continuum and "5" the furthest from the fractures, or the inner-most matrix continuum. It can be seen that the MINC model can correctly represent both the front propagation through the fractured network system (Fig. 6 (a-c)) and the infiltration into the matrix blocks (Fig. 6 (d-f)). At steady state the non-wetting saturations of the two models converge to the same value and are in perfect agreement (Fig. 6f).

4.1.2 Test problem 2: Quarter five-spot problem

For the second test we use the same fracture network system as in the previous example. We consider a contamination spill of TCE (D-NAPL) from a point source which is infiltrating into a fractured ground water reservoir (Fig. 7). This is similar to a quarter five-spot problem, commonly encountered in reservoir engineering. In comparison to the previous test, the location of the source and the fracture configuration leads to an anisotropic permeability tensor which should be captured by the upscaled MINC model. We also include the influence of capillary forces and we concentrate on the effect of the entry pressure which is used both for the fine- and the coarse-scale models. Voluntarily, the capillary pressure saturation $p_c - S_w$ curves are chosen close to each other: entry pressure in the matrix $p_d = 1200$ $[Pa]$ and entry pressure in the fracture $p_d = 1000$ $[Pa]$. To keep the problem simple and maintain the focus on the entry pressure effect we consider that the porosities of the two materials are the same (Tab. 2).

The boundary conditions are set to no-flow on all boundaries except the lower left

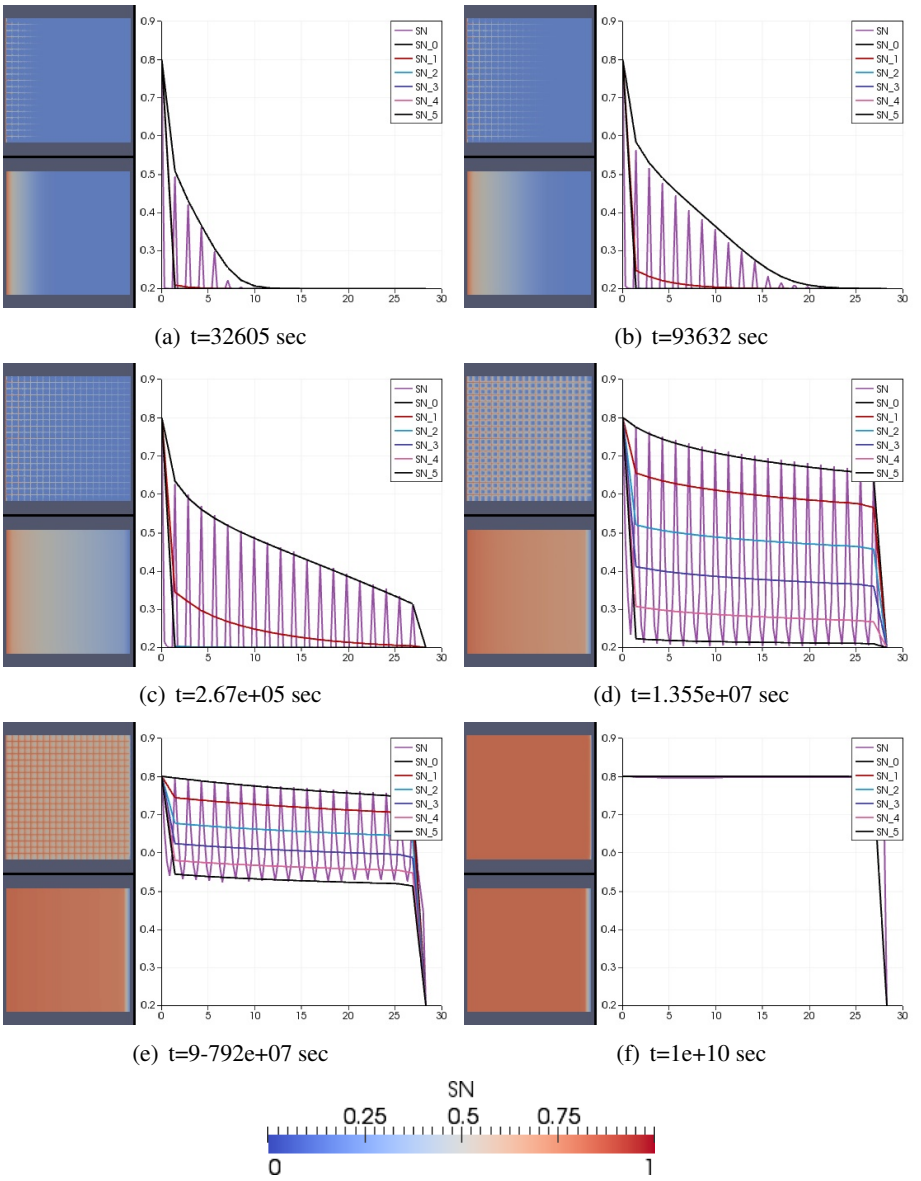

(a) t=32605 sec (b) t=93632 sec

(c) t=2.67e+05 sec (d) t=1.355e+07 sec

(e) t=9-792e+07 sec (f) t=1e+10 sec

Figure 6: Permeameter type example: Non-wetting phase saturation profiles plotted over the diagonal. The upper left plot in each subfigure represents the spatial saturation distributions obtained with the reference DFM model (*SN* curve), while the lower left plot is the extended MINC model (*SN*_0 is fracture continuum, *SN*_1 matrix continuum 1,etc.).

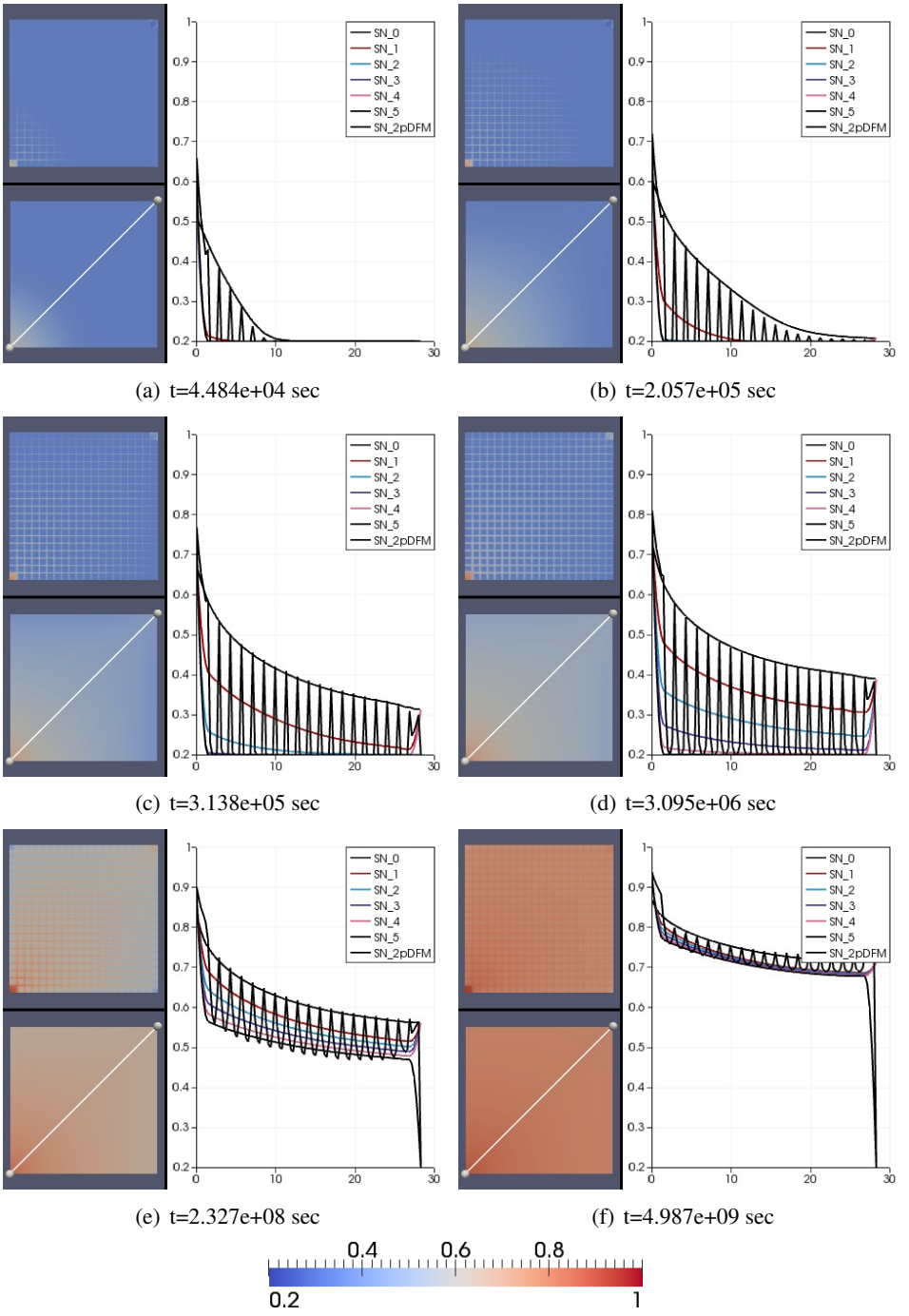

(a) t=4.484e+04 sec (b) t=2.057e+05 sec

(c) t=3.138e+05 sec (d) t=3.095e+06 sec

(e) t=2.327e+08 sec (f) t=4.987e+09 sec

Figure 7: Quarter five spot example: non-wetting saturation profiles plotted over the diagonal line (white color) at different time steps. The DFM spatial distributions of saturations (*SN* curve) is plotted in the upper left part of each subfigure above the MINC (*SN*_0, *SN*_1, ..,*SN*_6).

Table 2: Material properties and problem description for "Quarter Five-spot" experiment.

		Domain Properties	
		matrix	**fracture**
Permeability, K	$[m^2]$	$1.0e-15$	$b^2/12$
Eff. porosity, ϕ	[-]	0.5	0.5
Entry pressure, p_d	$[Pa]$	1200	1000
Pore size dist. idx.λ	[-]	0.5	0.5
Residual saturation S_{wr}	[-]	0.01	0.01
Residual saturation S_{nr}	[-]	0.01	0.01
Fracture aperture b	$[m]$	-	$3.915e-4$
		Fluid Properties	
Viscosity Water, μ_w	$[kg/ms]$	$1.0e-3$	
Density Water, ρ_w	$[kg/m^3]$	1000	
Viscosity DNAPL, μ_n	$[kg/ms]$	$5.7e-4$	
Density DNAPL, ρ_n	$[kg/m^3]$	1460	
		Boundary Conditions	
LowerLeft[Neumann]:			
q_w , q_n	$[kg/ms]$	$q_w = 0$	$q_n = 2.0e-02$
UpperRight[Dirichlet]:			
p_w , S_n	$[Pa]$, [-]	$p_w = 1.0e+05$	$S_n = 0.20$
ELSE [No Flow]			
		Initial Conditions	
p_w , S_n	$[Pa]$, [-]	$p_w = 1.0e+05$	$S_n = 0.2$

corner where a constant injection rate of non-wetting phase 2.0e-2 kg/s.m is chosen, and the upper right corner, Dirichlet, with p_w=1.0e5 $[Pa]$ and S_n=0.2, which are also the initial values inside the domain. The coarse blocks of the MINC model are subgridded with a number of 6 continua. The dimensions in the determination of the upscaled effective parameters are the same as in the "Permeameter" example, i.e. 2 $\times$ 2 meters. Also for this case, it can be seen that the MINC model can accurately represent the front propagation (Fig. 7 (a-c)) as well the infiltration into the matrix blocks, which starts occurring when the matrix entry pressure is overcome (Fig. 7 (d-f)). The non-wetting saturation profiles plotted over the diagonal line show that the fracture continuum always fits the peaks of the DFM model. Considering the observation of Zimmerman, Hadgu, and Bodvarsson (1996) the MINC approach

should be employed with matrix blocks discretized into ten or more nested continua. For the previous examples, we have performed a sensitivity analysis using different infiltration rates, finer or coarser discretizations and different numbers of interacting continua for the coarse blocks. The DFMs can be accurately approximated with an upscaled MINC model having a coarse grid refinement of 10×10 and a subgridding of 3 nested volume elements.

4.2 Test problem 3: Two-phase flow in a layerd fractured carbonate model BED3

In the following example we present a naturally fractured domain, having the patterns mapped on a wave platform along the southern margin of the Bristol Channel coast, United Kingdom. The geometry has previously been investigated with the numerical framework complex system platform (CSP) BED3 [Belayneh, Masihi, Matthai, and King (2006)] and later in several single- and multi-phase problems [Geiger, Cortis, and Birkholzer (2010); Geiger and Emmanuel (2010); Matthai, Nick, Pain, and Neuweiler (2010)]. Domain dimensions are 18 x 8 m^2 (Fig. 8) and it mainly consists of limestone rocks interbedded with shales having vertical joints that connect the horizontal fractures. The reservoir is represented in high detail and has a strong fracture connectivity. The material parameters for both matrix and the fracture domains are given in Tab. 3. We employ the same capillary-pressure-saturation curves as in the "quarter five-spot" example but this time we consider that fractures and matrix have different porosities, i.e. 0.9 for fractures and 0.3 for the rock matrix.

For this example, we are using two fluids with considerably different viscosities: water and air. The boundary and initial conditions are the same as in Test problem 1: on the left boundary p_w = 2.0e+05 [*Pa*] and the S_n = 0.80, on the right boundary p_w = 1.0e+05 [*Pa*] and S_n = 0.20, and the top and bottom boundaries are set no-flow; initial conditions: non-wetting saturation S_n = 0.20 and a wetting pressure, p_w = 1.0e+05 [*Pa*]. In the preprocessing step, the geometry of the fracture system is given as a CAD format. We generate the finite element grid with `ICEM` and convert the mesh file using `csp2art` into "*.net*". We use this geometry to calculate the reference solution with `2pDFM` simulator. For the `2pMINC` model, another geometry file consisting only of the fracture system is created. The file is converted to *.art* and the coarse grid mesh is overlapped on the fracture network (Fig. 8 upper). The vertical and horizontal new inner lines are assigned with boundary ids bigger than one, which ensures that the fracture mapper (`artreader`) will recognize them as non-fractures. Using `ART3D` we create an adaptive mesh with higher refinement around the fractures as illustrated by Fig. 8 (lower). The next step is the creation of the UG grid readable by DuMu^x and mapping of each individual fracture. The

Table 3: Material properties and problem description for "Bristol" experiment.

		Domain Properties	
		matrix	**fracture**
Permeability, K	$[m^2]$	$1.0e-15$	$b^2/12$
Eff. porosity, ϕ	[-]	0.3	0.9
Entry pressure, p_d	$[Pa]$	1200	1000
Pore size dist. idx.λ	[-]	0.5	0.5
Residual saturation S_{wr}	[-]	0.0	0.0
Residual saturation S_{nr}	[-]	0.0	0.0
Fracture aperture b	$[m]$	-	$3.915e-4$
Temperature T	$[^\circ K]$	293.15	293.15
		Fluid Properties	
Viscosity Water, μ_w	$[kg/ms]$	$1.0e-3$	
Density Water, ρ_w	$[kg/m^3]$	1000	
Viscosity Air, μ_n	$[kg/ms]$	$f(p,T) \approx 1.6e-5$	
Density Air, ρ_n	$[kg/m^3]$	$\frac{p_n M}{RT}$	
		Boundary Conditions	
Left[Dirichlet]:			
p_w , S_n	$[Pa]$, [-]	$p_w = 2.0e+05$	$S_n = 0.80$
Right[Dirichlet]:			
p_w , S_n	$[Pa]$, [-]	$p_w = 1.0e+05$	$S_n = 0.20$
ELSE [No Flow]			
		Initial Conditions	
p_w , S_n	$[Pa]$, [-]	$p_w = 1.0e+05$	$S_n = 0.20$

coarse blocks chosen for the calculation of the effective parameters are 2×2 meters (Fig. 8) each containing a number of 6 nested volume elements. After solving the single phase flow problems between the coarse blocks the inter-coarse-block effective permeabilities result ranging between 2.42e-12 and 4.78e-12 m^2. These parameters are given to the `2pMINC` flow simulator for the processing step.

In Fig. 10 we can see as in the previous examples, that the model predicts the saturation distributions for the whole simulation spectrum correctly (front arrival to the other boundary, non-wetting phase infiltration into the matrix blocks and until the steady sate). As the fracture system is not periodic, the fracture continuum curve *SN*_0 of the MINC model is not touching all the peaks but it gives a reasonably good approximation. This is also valid for all the rock matrix continua

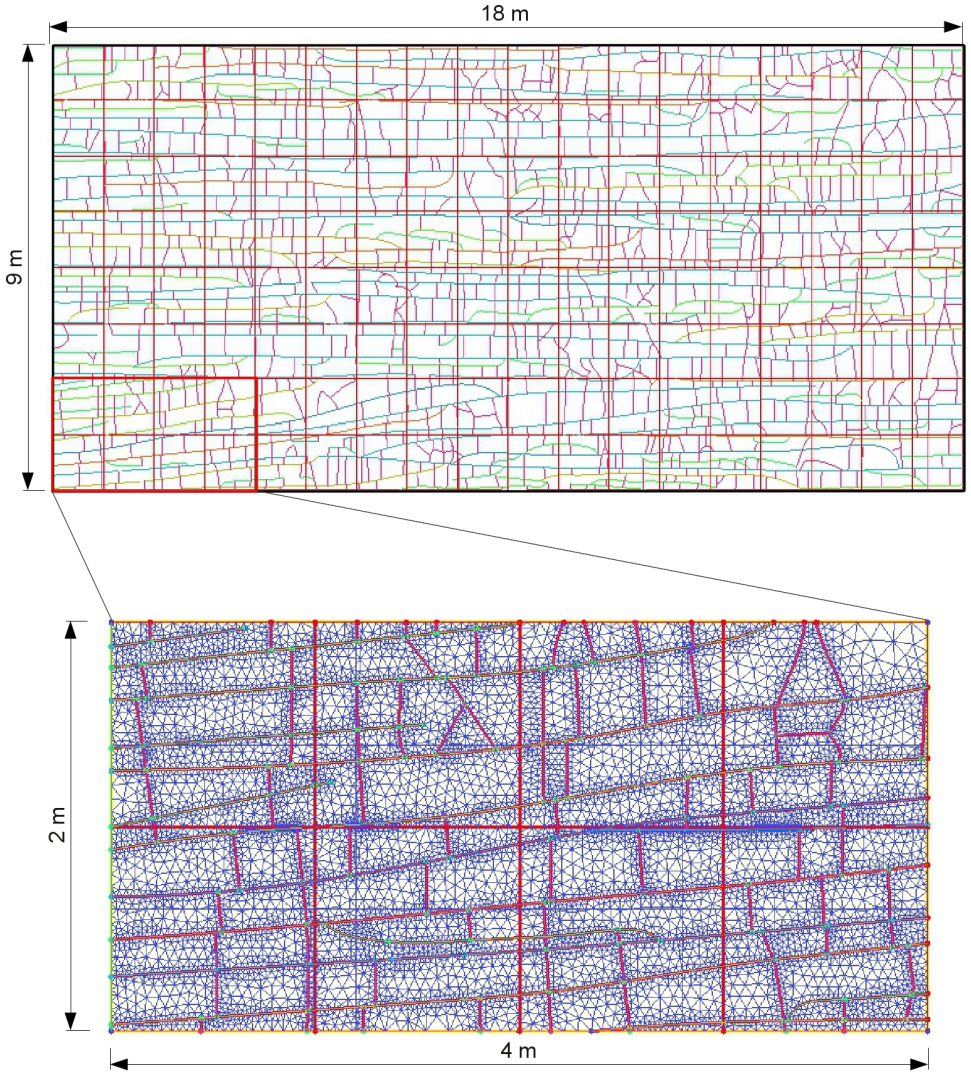

Figure 8: Test problem 3: Domain description and an example for the subdivision of the Bristol fracture system in coarse blocks (two cells) and their unstructured gridding.

which remain in between the saturation limits obtained with the discrete model. As expected, the fractures dominate flow and the non-wetting front travels very fast through the fracture network to the left boundary (Fig. 10 (a-c)). Next, it starts infiltrating into the rock blocks (Fig. 10 (c-e)), until the steady state is reached

(Fig. 10(f)). The saturation in the fracture domain both in the DFM and the MINC model reach the value 0.8 while in the matrix they are slightly smaller 0.78. With

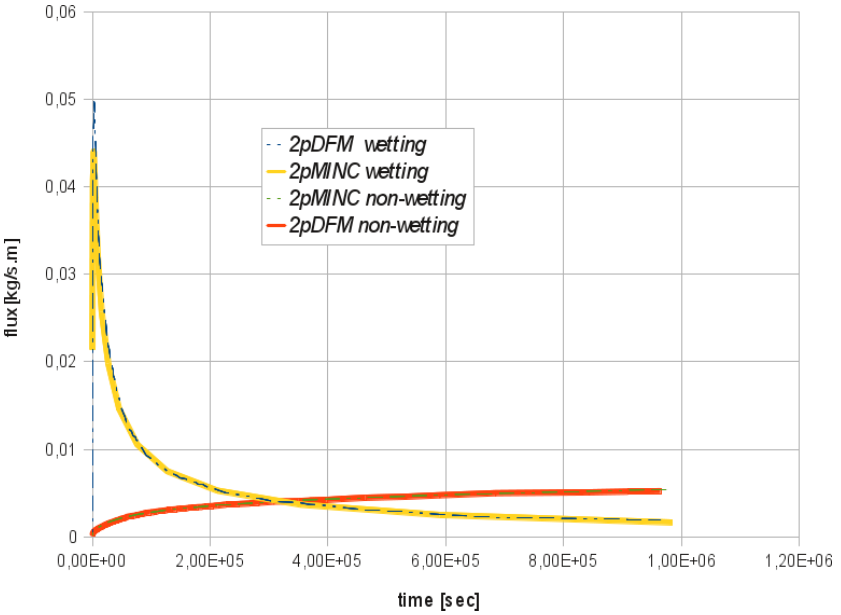

Figure 9: Test problem 3: Mass fluxes of wetting and non-wetting phase plotted over time at line (x = 1.8m) obtained with 2pDFM and 2pMINCsimulators

the result visualization step we have successfully closed the last cycle in the workflow. The simulation environment is practical and flexible as it allows the user to choose between accuracy and computational speed. Another point for flexibility is the ability to manipulate the geometries with our developed software as well as more productive commercial tools. 2pMINC model correctly reproduces not only the saturation profiles, but also the mass fluxes (Fig. 9) and is able to capture the capillary effects. It shows a good accuracy and a very good efficiency in computation speed. Tab. 4 compares the simulation times for the 2pDFM and 2pMINC, together with the number of elements and vertices.

5 Summary and Conclusion

We have developed a practical tool to simulate two phase flow in large-scale fractured reservoirs. The simulation method is general because it allows handling of densely fractured systems with irregular geometries as well as of the regions where fractures have lower connectivity. It is also flexible because it benefits from both

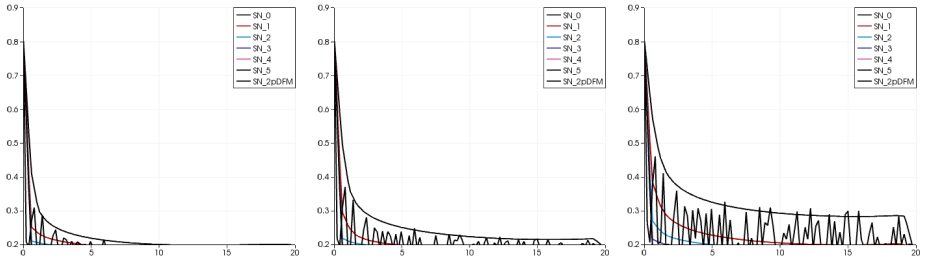

(a) t=2541.7 sec (b) t=9117.8 sec (c) t=2541.7 sec

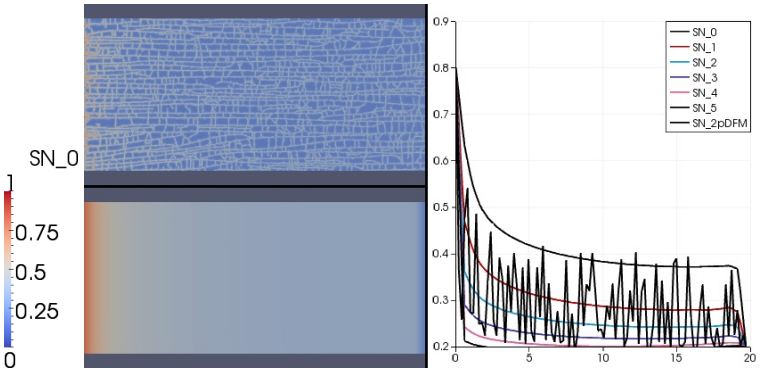

(d) t=2541.7 sec

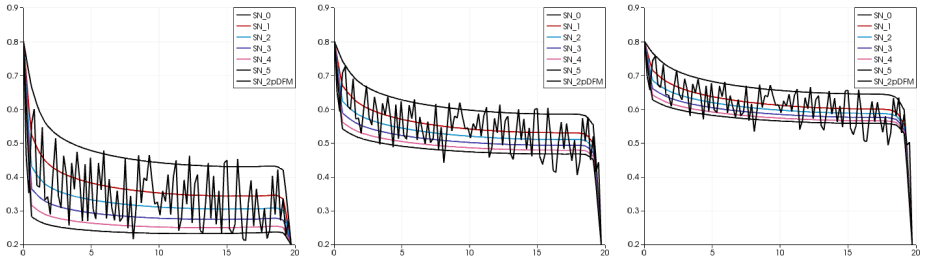

(e) t=5.90e+05 sec (f) t=7.521+06 sec (g) t=2.0167+07 sec

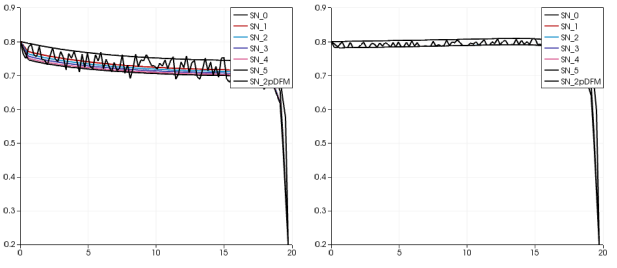

(h) t=2.0167+07 sec (i) steady state

Figure 10: Test problem 3: Non-wetting saturation profiles plotted over the diagonal for Bristol Channel fractured reservoir analogue

Table 4: Simulation times and grid specifications for the numerical experiments

Experiment	Model	Vertex No	Element No	Sim. Time [sec]
Ex.1: Permeameter	2pDFM	37269	73847	15517.6
	2pMINC	11×11	10×10	421.3
Ex.2: Fivespot	2pDFM	37269	73847	122483.6
	2pMINC	11×11	10×10	2046
Ex.3: Bristol	2pDFM	42490	84348	331364
	2pMINC	19×9	18×8	180

the fracture complexity of the DFM and the computational simplicity of the CFM, which is a compromise between accuracy and computation speed. Considering the advantage of the extended MINC method over the classical MINC method (like Pruess (1992)) which is the derivation of the effective parameters from detailed hydrodynamic and geometric properties of the fracture system, we have introduced a workflow for efficient solving of two-phase flow in fractured porous media. It starts with the geometrical modeling of the fracture network system which is/can be created with a geostatistical fracture generator, then the generation of the optimal fine- and coarse-mesh, and ends with the numerical simulator and the post-processing. The tests showed that the 2pMINC simulator can represent the fluxes and saturation profiles obtained with the discrete 2pDFM simulator, giving very good speedup factors. We can also conclude that both the matrix-fracture transfer and entry pressure effects are correctly estimated and are based on a physical approach. It is clear that if geologic data are available the most accurate solutions are obtained with a DFM approach. Considering the increase in computational power and the possibility of doing multiple core calculations this may represent the best choice for the future, however an accurate, practical tool based on a generalized double porosity concept with high flexibility still remains a good alternative.

Acknowledgement: This work was funded by the German Federal Ministry of Education and Research (BMBF) through the IPSWaT programme. We thank Sebastian Geiger for providing the Bristol BED3 geometry and Sorin Pop for reviewing this work.

References

Abushaikha, A.; Gosselin, O. (2009): SubFace Matrix-Fracture transfer function: Improved model of gravity drainage/ imbibition. In *Proceedings of EUROPEC/EAGE Conference and Exhibition*.

Assteerawatt, A. (2008): *Flow and Transport Modelling of Fractured Aquifers based on Geostatistical Approach*. PhD thesis, Institute of Hydraulic Engineering, Stuttgart, Germany, 2008.

Barenblatt, G. I.; Zheltov, I. P.; Kochina, I. N. (1960): Basic concepts in the theory of seepage of homogeneous liquids in fissured rocks [strata]. *Journal of Applied Mathematics and Mechanics*, vol. 24, no. 5, pp. 1286–1303.

Basquet, R.; Bourbiaux, B.; Cohen, C. (2005): Fracture flow property identification: An optimized implementation of discrete fracture network models. In *Proceedings of SPE Middle East Oil and Gas Show and Conference*.

Bastian, P.; Birken, K.; Johannsen, K.; Lang, S.; Neuss, N.; Rentz-Reichert, H.; Wieners, C. (1997): UG - a flexible software toolbox for solving partial differential equations. *Computing and Visualization in Science*, vol. 1, pp. 27–40.

Belayneh, M.; Masihi, M.; Matthai, S. K.; King, P. R. (2006): Prediction of vein connectivity using the percolation approach: model test with field data. *Journal of Geophysics and Engineering*, vol. 3, no. 3, pp. 219–229.

Berkowitz, B. (2002): Characterizing flow and transport in fractured geological media: A review. *Advances in Water Resources*, vol. 25, no. 8-12, pp. 861–884.

Bodvarsson, G. S.; Boyle, W.; Patterson, R.; Williams, D. (1999): Overview of scientific investigations at yucca mountain–the potential repository for high-level nuclear waste. *Journal of Contaminant Hydrology*, vol. 38, no. 1-3, pp. 3–24.

Bourbiaux, B.; Cacas, M.; Sarda, S.; Sabathier, J. (1997): A fast and efficient methodology to convert fractured reservoir images into a Dual-Porosity model. *Society of Petroleum Engineers*.

Brooks, R. H.; Corey, A. T. (1964): Hydraulic properties of porous media. *Hydrology Paper No. 3*, , no. Colorado State University, Fort Collins, Colorado.

Carneiro, J. F. (2009): Numerical simulations on the influence of matrix diffusion to carbon sequestration in double porosity fissured aquifers. *International Journal of Greenhouse Gas Control*, vol. In Press, Corrected Proof.

Dedner, A. (2004): A parallel, load-balanced MHD code on locally-adapted, unstructured grids in 3d. *Computing and Visualization in Science*, vol. 7, pp. 79–96.

Douglas, J. J.; Arbogast, T. (1990): Dual porosity models for flow in naturally fractured reservoirs. *In Cushman, H. (Ed.) Dynamics of fluids in hierarchical porous media*.

Duijn, C. J.; Molenaar, J.; Neef, M. J. (1995): The effect of capillary forces on immiscible two-phase flow in heterogeneous porous media. *Transport in Porous Media*, vol. 21, no. 1, pp. 71–93.

Famy, C.; Bourbiaux, B.; Quintard, M. (2005): Accurate modeling of Matrix-Fracture transfers in Dual-Porosity models: Optimal subgridding of matrix blocks. In *Proceedings of SPE Reservoir Simulation Symposium*.

Flemisch, B.; Darcis, M.; Erbertseder, K.; Faigle, B.; Lauser, A.; Mosthaf, K.; Müthing, S.; Nuske, P.; Tatomir, A.; Wolff, M.; Helmig, R. (2011): DuMux: DUNE for multi-phase, component, scale, physics, ... flow and transport in porous media. *Advances in Water Resources*, vol. In Press, Corrected Proof.

Flemisch, B.; Fritz, J.; Helmig, R.; Niessner, J.; Wohlmuth, B. (2007): DUMUX: a multi-scale multi-physics toolbox for flow and transport processes in porous media. *ECCOMAS Thematic Conference on Multi-scale Computational Methods for Solids and Fluids*.

Fuchs, A. (2001): Almost regular triangulations of trimmend NURBS-Solids. *Engineering with Computers*, vol. 17, no. 1, pp. 55–65.

Geiger, S.; Cortis, A.; Birkholzer, J. T. (2010): Upscaling solute transport in naturally fractured porous media with the continuous time random walk method. *Water Resources Research*, vol. 46, pp. 13 PP.

Geiger, S.; Emmanuel, S. (2010): Non-Fourier thermal transport in fractured geological media. *Water Resources Research*, vol. 46, pp. 13 PP.

Gong, B.; Karimi-Fard, M.; Durlofsky, L. (2008): Upscaling discrete fracture characterizations to Dual-Porosity, Dual-Permeability models for efficient simulation of flow with strong gravitational effects. *SPE Journal*, vol. 13, no. 1.

Helmig, R. (1997): *Multiphase Flow and Transport Processes in the Subsurface: A Contribution to the Modeling of Hydrosystems*. Springer, 1 edition.

Hemminger, A. (2002): *Modellierung von Kluftaquifersystemen: Geostatistische Analyse and deterministisch-stochastische Kluftgenerierung*. PhD thesis, Stuttgart, 2002.

Karimi-Fard, M.; Durlofsky, L. J.; Gong, B. (2006): Generation of coarse-scale continuum flow models from detailed fracture characterizations. *Water Resources Research*, vol. 42, pp. W10423.

Kazemi, H. (1976): Numerical simulation of Water-Oil flow in naturally fractured reservoirs. *Society of Petroleum Engineers*, vol. 16, no. 6, pp. 317–326.

Kopp, A.; Class, H.; Helmig, R. (2009): Investigations on CO2 storage capacity in saline aquifers: Part 1. dimensional analysis of flow processes and reservoir

characteristics. *International Journal of Greenhouse Gas Control*, vol. 3, no. 3, pp. 263–276.

Lemonnier, P.; Bourbiaux, B. (2010): Simulation of naturally fractured reservoirs. state of the art - part 2 - Matrix-Fracture transfers and typical features of numerical studies. *Oil & Gas Science and Technology - Revue de l'Institut Français du Pétrole*, vol. 65, no. 2, pp. 24.

Lewandowska, J.; Szymkiewicz, A.; Burzynski, K.; Vauclin, M. (2004): Modeling of unsaturated water flow in double-porosity soils by the homogenization approach. *Advances in Water Resources*, vol. 27, no. 3, pp. 283–296.

Matthai, S. K.; Nick, H. M.; Pain, C.; Neuweiler, I. (2010): Simulation of solute transport through fractured rock: A Higher-Order accurate Finite-Element Finite-Volume method permitting large time steps. *Transport in Porous Media*, vol. 83, pp. 289–318.

Min, K.; Jing, L.; Stephansson, O. (2004): Determining the equivalent permeability tensor for fractured rock masses using a stochastic REV approach: Method and application to the field data from sellafield, UK. *Hydrogeology Journal*, vol. 12, no. 5, pp. 497–510.

Naimi-Tajdar, R.; Han, C.; Sepehrnoori, K.; Arbogast, T.; Miller, M. (2007): A fully implicit, compositional, parallel simulator for IOR processes in fractured reservoirs. *SPE Journal*, vol. 12, no. 3.

Neuman, S. P. (2005): Trends, prospects and challenges in quantifying flow and transport through fractured rocks. *Hydrogeology Journal*, vol. 13, no. 1, pp. 124–147.

Niessner, J.; Helmig, R.; Jakobs, H.; Roberts, J. (2005): Interface condition and linearization schemes in the newton iterations for two-phase flow in heterogeneous porous media. *Advances in Water Resources*, vol. 28, no. 7, pp. 671–687.

Pruess, K. (1992): Brief guide to the MINC-Method for modeling flow and transport in fractured media. *Tech. Rep. LBNL-32195 Lawrence Berkeley National Laboratory*.

Pruess, K.; Narasimhan, T. N. (1982): A practical method for modeling fluid and heat flow in fractured porous media. *Society of Petroleum Engineers*, vol. 25, pp. 14–26.

Reichenberger, V.; Jakobs, H.; Bastian, P.; Helmig, R. (2006): A mixed-dimensional finite volume method for two-phase flow in fractured porous media. *Advances in Water Resources*, vol. 29, no. 7, pp. 1020–1036.

Sarda, S.; Jeannin, L.; Basquet, R.; Bourbiaux, B. (2002): Hydraulic characterization of fractured reservoirs: Simulation on discrete fracture models. *SPE Reservoir Evaluation & Engineering*, vol. 5, no. 2.

Schmidt, A.; Siebert, K. G. (2005): *Design of adaptive finite element software: the finite element toolbox ALBERTA*. Springer.

Unsal, E.; Matthäi, S. K.; Blunt, M. J. (2009): Simulation of multiphase flow in fractured reservoirs using a fracture-only model with transfer functions. *Computational Geosciences*, vol. 14, no. 4, pp. 527–538.

Vitel, S.; Souche, L. (2007): Unstructured upgridding and transmissibility upscaling for preferential flow paths in 3D fractured reservoirs. In *Proceedings of SPE Reservoir Simulation Symposium*.

Warren, J.; Root, P. (1963): The behaviour of natuarally fractured reservoirs. *Society of Petroleum Engineers*, vol. 228, pp. 245 – 255.

Wu, Y.; Pan, L.; Pruess, K. (2004): A physically based approach for modeling multiphase fracture-matrix interaction in fractured porous media. *Advances in Water Resources*, vol. 27, no. 9, pp. 875–887.

Zimmerman, R. W.; Bodvarsson, G. S. (1995): Effective block size for imbibition or absorption in dual-porosity media. *Geophysical Research Letters*, vol. 22, no. 11, pp. 1461–1464.

Zimmerman, R. W.; Chen, G.; Hadgu, T.; Bodvarsson, G. S. (1993): A numerical dual-porosity model with semianalytical treatment of fracture/matrix flow. *Water Resources Research*, vol. 29, no. 7, pp. PP. 2127–2137.

Zimmerman, R. W.; Hadgu, T.; Bodvarsson, G. S. (1996): A new lumped-parameter model for flow in unsaturated dual-porosity media. *Advances in Water Resources*, vol. 19, no. 5, pp. 317–327.

Zyvoloski, G. A.; Robinson, B. A.; Viswanathan, H. S. (2008): Generalized dual porosity: A numerical method for representing spatially variable sub-grid scale processes. *Advances in Water Resources*, vol. 31, no. 3, pp. 535–544.